

# Elastic instability in a straight channel of viscoelastic flow without prearranged perturbations

Yuke Li<sup>1</sup> and Victor Steinberg<sup>1,2</sup>

<sup>1</sup>*Department of Physics of Complex Systems, Weizmann Institute of Science, Rehovot 7610001, Israel*

<sup>2</sup>*The Racah Institute of Physics, Hebrew University of Jerusalem, Jerusalem 91904, Israel*

(Dated: January 20, 2022)

We report experimental results on elastic instability in a viscoelastic channel shear flow due to only a natural non-smoothed inlet and small holes along the channel for pressure measurements. We show that non-normal mode instability results in elastic waves and chaotic flow self-organized into periodically cycled stream-wise streaks synchronized by elastic wave frequency. The chaotic flow persists above the transition with increasing  $Wi$  further into elastic turbulence and drag reduction regimes. Thus, we resolve the recent puzzle whether strong prearranged perturbations are necessary to get an elastic instability in parallel shear viscoelastic flow. Moreover, flow resistance, velocity spectra decay, and elastic wave speed reveal the same scaling with  $Wi$  as obtained in the case of strong disturbances. The remarkable result is that the all scaling behavior and streaks are found in the entire channel with small attenuation, in a sharp contrast to the flow with strong prearranged perturbations.

In parallel shear Newtonian flows, turbulence emerges at the high Reynolds numbers ( $Re$ ) due to inertial stresses, whereas for low  $Re$ , they are dominated by viscous dissipation and remain laminar. In contrast, in viscoelastic fluid flows with curved streamlines, at  $Re \ll 1$  and the high Weissenberg number,  $Wi$ , a linear elastic instability due to a single fastest growing mode results in a single most stable mode, which leads to elastic turbulence (ET) at vanishing inertia, as  $Wi$  is increased further. ET is an inertia-less, chaotic flow driven purely by elastic stress generated by polymers stretched by the flow. The latter is modified by a feedback reaction of the elastic stress. As the result, the elastic "hoop" stress, generated by polymers stretched along the curved streamlines, engenders a force towards the curvature center, which triggers an elastic instability [1, 2] and ET at  $Wi \gg 1$  and  $Re \ll 1$  [3–5]. The elastic instability mechanism becomes ineffective in zero curvature limit [1, 6], in such as parallel shear flows, where their linear stability in the whole range of  $Wi$  is proved [7, 8], similar to Newtonian parallel shear flows. Here  $Wi = \lambda U/h$  defines the degree of polymer stretching [9],  $Re = \rho U h / \eta$ , where  $U$  is the mean flow velocity,  $\lambda$  is the longest polymer relaxation time,  $\rho, \eta$  are the solution density and dynamic viscosity, respectively, and  $h$  is the characteristic vessel scale.

Parallel shear flows of viscoelastic fluids are proved to be linearly stable at all  $Wi$  [7, 8], though it does not imply their global stability. Indeed, two recent theoretical developments [10–14] suggest two different possible mechanisms of instability of parallel shear viscoelastic flows. In spite of different nature of these mechanisms, namely normal versus non-normal unstable modes, both mechanisms consider finite-size perturbations as a necessary condition for the instability. First mechanism is based on a hysteretic, sub-critical finite-amplitude bifurcation, based on a nonlinear extension of the normal mode linear stability analysis, predicts a single normal mode, namely

2D traveling waves, growing exponentially and saturated at a sufficiently large amplitude, which at higher  $Wi$  may result in ET [10]. The second approach utilizes theoretically and verified experimentally a non-modal analysis of linearly stable shear Newtonian flows at  $Re \gg 1$  [15–18]. This approach used in theory and numerical simulations for the non-modal instability of viscoelastic channel and plane Couette flows at  $Wi \gg 1$  and  $Re \ll 1$  (and the elasticity number  $El = Wi/Re \gg 1$ ) is introduced in Refs. [11–13]. The resulting span-wise modulated coherent structures are revealed in plane Couette and channel flows of visco-elastic fluids [11–14]. The elastic instability in viscoelastic parallel shear flows is considered to occur via transient stream-wise streaks generated by weakly unstable stream-wise vortices [13, 14]. Both coherent structures (CSs) are the most amplified, similar to those observed in Newtonian shear flows at  $Re \gg 1$  [17, 18]. Since the theory is based on the linearized equations for the non-normal pseudo-modes, it describes only the linear transient stages of the instability and cannot predict CSs prevailed in at saturation due to nonlinear interactions. In the present study, we show how the nonlinear interactions stabilize CSs selected by the linearized dynamics and eventually promote transition to ET at higher  $Wi$ .

Recent experiments in pipe [19] and straight square micro-channel [20–22] with large prearranged perturbations, generated either by the jet [19] or the obstacle array located at the inlet [20], reveal an elastic instability directly into chaotic flow characterized by continuous velocity and pressure power spectra. Moreover, the authors of Ref. [20] claim observing a hysteresis in the transition suggested in Ref. [10]. However, the predicted backward instability results in the most unstable normal mode that is a 2D traveling wave, which is not detected in the experiment. These experimental results suggest that the elastic instability and probably ET may occur in parallel

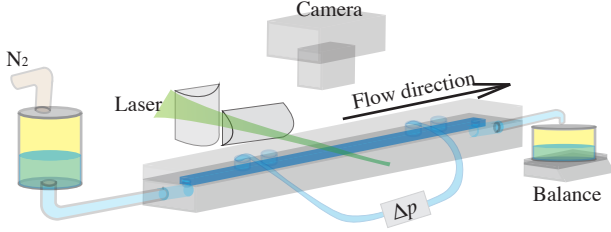


FIG. 1. Schematics of experimental setup. Four instead of six holes are drawn for simplicity.

shear viscoelastic flows, through a direct transition to a chaotic states with a large number of the excited modes observed experimentally in both parallel shear viscoelastic flows inconsistent with a normal mode instability [19–21].

Recently, a non-modal instability in a parallel shear channel flow is confirmed in a straight channel with strong perturbations at the inlet [23, 24], as suggested in Ref. [11–14]. Furthermore, elastic waves and chaotic flow, observed only in a part of the channel, adjacent to the perturbation source, are self-organized into regularly cycled stream-wise vortices and streaks synchronized by elastic wave frequency in all three flows regimes [23]. Throughout the rest of a channel flow, elastic waves and CSs decay, with normalized perturbation intensity that reduces from roughly 10% down to 4% downstream until the outlet [23].

In this Letter, we present results that answer two questions, namely: (i) Whether three different chaotic flow regimes, occurred above an elastic instability as the result of finite-size perturbations due to a non-smoothed inlet and six small holes, exhibit the same scaling of the flow properties and elastic wave speed with  $Wi$ , as observed in the flow with strong prearranged perturbations [23, 24]; and (ii) Either these chaotic flows are self-organized into periodically cycled CSs, stream-wise rolls and streaks synchronized by elastic wave frequency or only into stream-wise streaks, similar to Ref. [25]. The key observation is that the scaling behavior in three flow regimes and streaks are found in the entire channel with small attenuation, in a sharp contrast to Refs. [23, 24].

The experiments are conducted in a straight long channel, with dimensions  $500(L) \times 3.5(w) \times 0.5(h)$  mm<sup>3</sup>, shown in Fig.1. The only main possible source of flow disturbances is the channel's non-smoothed inlet and six holes in the top plate for pressure measurements. As the working fluid, we use the polymer solution prepared viscous aqueous solvent with 64% sucrose with dissolved high-molecule-weight Polyacrylamide (PAAm, Polysciences,  $M_w = 18MDa$ ) at a dilute concentration of 80ppm. The solution properties are the solution density  $\rho = 1320$  kg/m<sup>3</sup>, the solvent and solution viscosity  $\eta_s = 0.13$  Pa·s and  $\eta = \eta_s + \eta_p = 0.17$  Pa·s, respectively,

$\eta_p/(\eta_s + \eta_p) \approx 0.3$ , where  $\eta_p$  is the polymer contribution into the solution viscosity, and the longest polymer relaxation time  $\lambda = 13$  s using the stress relaxation method [26].

The fluid in the channel is driven by N<sub>2</sub> gas by pressurized up to 100 psi. During experiments, we use a PC-interfaced balance (BPS-1000-C2-V2, MRC) to measure the time-averaged fluid mass discharge rate at the channel exit,  $Q = \langle \Delta m / \Delta t \rangle$ , where  $m(t)$  is weight instantaneously fluid as a function of time. Then the mean velocity is calculated as  $U = Q / \rho w h$ , and  $Wi = \lambda U / h$  and  $Re = \rho U h / \eta$ , which vary in the ranges (30, 6000) and (0.005, 0.9), respectively. We also measure pressure drops for flow resistance and fluctuations using high resolution differential pressure sensors of accuracy in various ranges: 5, 30, and 60 psi (HSC series, Honeywell).

We conduct measurements of the velocity field at various distances  $l/h$  downstream from the inlet, using the particle image velocimetry (PIV) method. For that we illuminate small latex particles (3.2 $\mu$ m fluorescent tracers with concentration  $\sim 0.67\%$  w/w, Latex Microsphere, Thermo Scientific) by a laser sheet with  $\sim 100\mu$ m thickness over the middle plane in the channel. Then we capture pairs of images of the tracers using high-speed (frame rate from 500 up to 8000) and high spatial resolution (up to 2048 $\times$ 2048 px<sup>2</sup>) camera (Mini WX100, Photron FASTCAM). The OpenPIV software [27] is employed to analyze  $u(x, z, t)$  and  $w(x, z, t)$  in 2D  $x$ - $z$  plane. We typically record data for periods of  $\sim \mathcal{O}(15)$  minutes or  $\sim \mathcal{O}(50\lambda)$  for each  $Wi$  to obtain sufficient statistics.

In Fig.2 (a) we present the measurements of the frictional drag as a function of  $Wi$  in high resolution presentation, where the friction factor,  $f/f_{lam}$ , is calculated as  $f = 2D_h \Delta P / \rho u_m^2 L_p$  and normalized by the laminar one  $f_{lam} \sim Re^{-1}$ . Here  $D_h = 2wh/(w+h) = 0.875$  mm is the hydraulic length,  $L_p = 270$  mm is the distance between two pressure measurement locations, and  $\Delta P$  is the pressure difference on the length  $L_p$ . In Fig.2 (b), we also measure pressure and velocity fluctuations to additionally characterize  $Wi_c$  and different flow regimes.

Four flow regimes are identified by different dependencies of  $f/f_{lam}$  on  $Wi$  (Fig.2 (a)). In a laminar flow the friction factor is independent on  $Wi$  and equal unity up to the elastic instability onset at  $Wi_c = 120 \pm 10$ . First,  $f/f_{lam}$  enhances with  $Wi$  as a power-law with an exponent  $0.10 \pm 0.03$ , followed by ET where it grows slower with the exponent  $0.06 \pm 0.02$ . And finally in drag reduction (DR) regime, the friction factor decays with the exponent  $-0.15 \pm 0.05$ . Thus, the dependence of  $f/f_{lam}$  on  $Wi$  reveals four flow regimes separated by three grey dashed lines in Fig.2.

Pressure fluctuations are normalized by pressure fluctuations in laminar flow, as  $p_{rms}/p_{rms, lam} - 1$ , as well as velocity fluctuations reduced by velocity fluctuations at laminar regime normalized by mean flow velocity, as  $(U_{rms} - U_{rms, lam})/U$  (Fig.2(b)). The velocity fluctuations

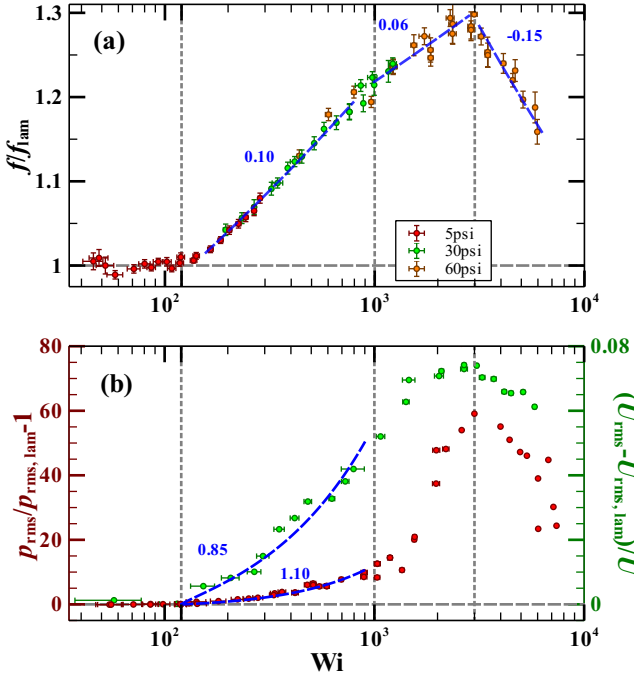


FIG. 2. (a) The friction factor ( $f/f_{lam}$ ) versus  $Wi$  in lin-log scales. Two individual pressure drop measurements are conducted at different positions but with the same gap: from  $l/h=185$  to  $725$  and from  $225$  to  $765$ , which are plotted together. Three differential pressure transducers in three ranges are used: 5 (in red), 30 (in green), and 60 (in orange) psi. (b) Normalized pressure ( $p_{rms}/p_{rms,lam} - 1$ ) and velocity ( $(U_{rms} - U_{rms,lam})/U$ ) fluctuations versus  $Wi$  in lin-log scales.

are measured at the center of middle plane via PIV. Analogously to the friction factor, both the normalized pressure and velocity fluctuations versus  $Wi$  disclose four flow regimes as well.  $p_{rms}/p_{rms,lam} - 1$  grows algebraically with an exponent of  $0.85 \pm 0.1$  and  $(U_{rms} - U_{rms,lam})/U$  with  $1.10 \pm 0.1$  above transition. These exponents differ from 0.5 indicating that the elastic instability is not a linear normal mode bifurcation [28].

Fig.3(a) presents energy spectra ( $E_u$ ) of stream-wise velocity versus normalized frequency ( $\lambda \cdot f$ ) at  $l/h=330$ , far downstream from the inlet, and the decay slopes are algebraically fitted. The slope exponents decrease from -1.2 to -2.8 in the transition regime, then further to -3.0 in ET, and finally increases back to -2.8 in DR. The chaotic continuous modes of power spectra just above the instability are another strong evidence of the non-modal nature of the elastically driven instability [12, 29, 30].

Using span-wise velocity energy spectra ( $E_w$ ) in lin-log scales (see an example in the inset in Fig.3(b)), we obtain the dependence of the elastic wave frequency on  $Wi$ , the first indication of the observation of elastic waves. The main proof of the elastic wave detection to be compared with our early observations [23–25, 31] is the result on the elastic wave speed ( $c_{el}$ ) scaling with  $(Wi - Wi_c)^\delta$ .

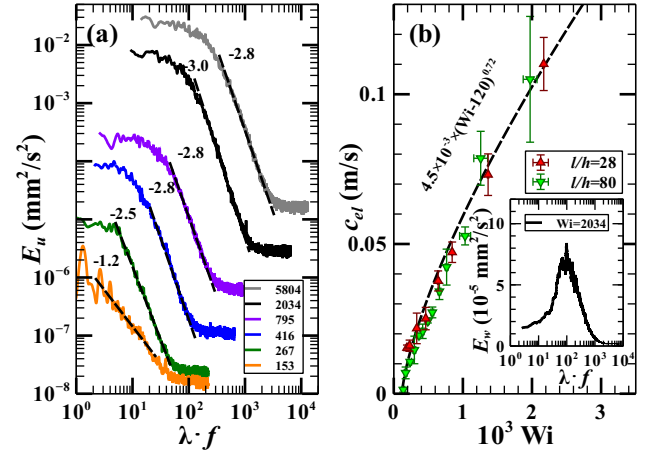


FIG. 3. (a) Energy spectrum of stream-wise velocity ( $E_u$ ) versus frequency normalized by  $\lambda$  at  $l/h=330$  in log-log scales. The velocity for each moment is measured at channel center. (b) Elastic wave speed ( $c_{el}$ ) versus  $Wi$  at  $l/h=28$  and 80 in lin-lin scales. The inset presents a peak of elastic wave in span-wise velocity energy spectrum ( $E_w$ ) at  $Wi = 2034$  at  $l/h=330$  in lin-log scales.

Fig.3(b) plots  $c_{el}$  vs  $Wi$  in lin-lin scales obtained by cross-correlation of velocity along stream-wise direction. By fitting the curve with  $c_{el} = A \times (Wi - Wi_c)^\delta$ , we obtain  $A = 4.5 \pm 0.5 \times 10^{-3}$  m/s and  $\delta = 0.72 \pm 0.02$ , which are the same as found in earlier flows: flows between two widely separated obstacles [31], and a straight channel with an array of obstacles at the inlet to excite strong perturbations [23, 24]. On the other hand, span-wise propagating elastic waves discovered in a straight channel with very weak perturbations generated by a small cavity in the top plate exhibit the coefficient  $A$  of about three orders of magnitude less and the same scaling exponent that maybe attributed to the strong span-wise confinement [25]. This suggests that the stream-wise-propagating elastic wave scaling relation with  $Wi - Wi_c$  could be universal.

To gain better insights into coherent states, we broaden the PIV window to the whole channel and at the stream-wise length  $\Delta l/h = 4$  to examine probable coherent states in this channel flow. As illustrated in Fig.4 from left to right in a single elastic wave cycle, at the beginning streaks first are self-organized with slightly perturbed interface that further is perturbed more and finally destroyed leading to a random flow at the end of the cycle. Then the next cycle starts. The streak dynamics is synchronized by elastic waves period. To prove experimentally the periodicity of a cycled self-sustained process with the period of the elastic waves we utilize the approach developed by us early to study the interface dynamics [23, 24] by examining a temporal evolution of  $\Delta u' = u'_2 - u'_1$ , the velocity fluctuation difference at two specific points across the interface, as shown in Fig. 5.

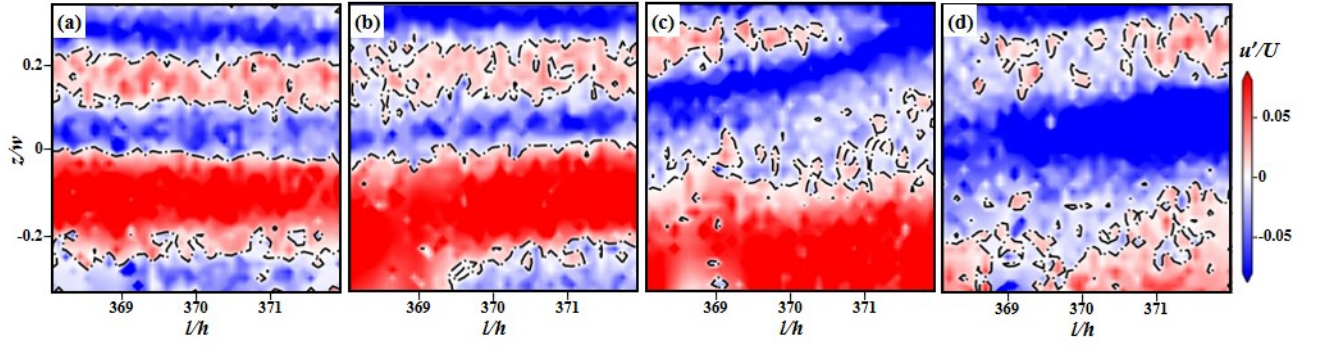


FIG. 4. Streak interface dynamics at  $l/h=330$  and  $Wi=2030$  in ET during a single cycle. The time-averaged stream-wise velocity profile is subtracted from the instant stream-wise velocity and normalized by time-averaged velocity  $u'/U$ . The black dashed line separates the low profile (blue) and high profile (red) streak interface. The moment  $t^* = t f_{el}$  of each image from left to right is 0.20, 0.38, 0.65, and 0.92. The interfaces of streaks are gradually interfered and break into random at the end of the cycle without any secondary instability.

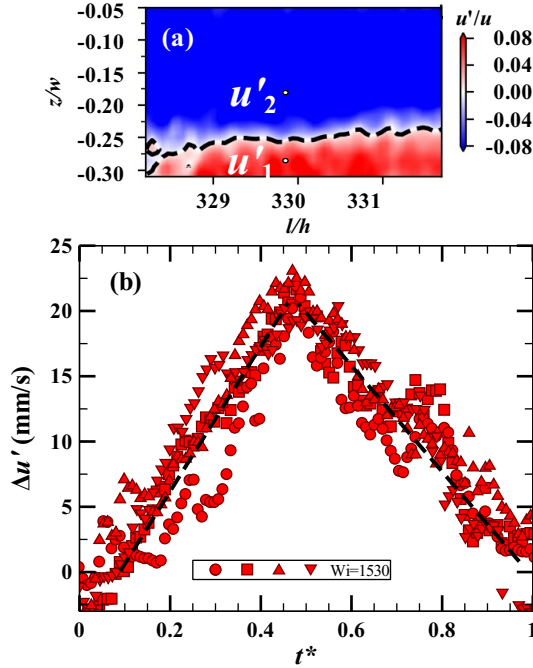


FIG. 5. Temporal dynamics of streaks at  $l/h=330$  at  $Wi=1530$ . (a) Span-wise-separated two points for calculation of  $\Delta u' = u'_2 - u'_1$ . (b) Four runs of  $\Delta u'$  for one cycle normalized by the period of elastic wave.

During each cycle,  $\Delta u'$  displays a non-monotonic temporal variation with the same peak values  $\Delta u'_{max}$  and cycle period. It should be pointed out that no secondary instability of the streaks such as the Kelvin-Helmholtz-like elastic instability is observed, which we attribute to lower intensity of the elastic waves compared to that found in Ref. [24].

To conclude, first of all, the main result of this study is resolving the recent puzzle whether strong prearranged perturbations are necessary to get an elastic instabil-

ity in parallel shear visco-elastic flows. Indeed, we investigate in a straight planar channel visco-elastic flow the elastically induced instability. In contrast to previously published works, we remove obstacles in the channel, while the non-smoothed inlet and six holes in the top plate along the channel provide perturbations that lead to the intrinsic non-modal instability at  $Wi_c = 120$ . We find and study four flow regimes: laminar, transitional, ET, and DR, which are characterized by measuring the friction factor, pressure and velocity fluctuations, and stream-wise velocity power spectra scaling. The velocity of stream-wise-propagating elastic wave shows the universal scaling relation with  $Wi - Wi_c$ . Using the approach to quantify a cycling period of streak dynamics [23, 24], we show that the period of the streak cycling dynamics is equal to the elastic wave period.

The remarkable and surprising finding is the existence of the streaks and elastic waves over the entire channel length up to  $l/h=980$ , in a sharp contrast with the case of the strong prearranged perturbations at the inlet [23, 24], where the CSs and elastic waves retain only in the short range of the channel from  $l/h = 36$  up to  $l/h \approx 200$ . Such distinct difference between two types of external perturbations may be explained by the following arguments. Finite-size perturbations are necessary to excite an intrinsic elastic instability in a channel flow. The presented above results of various measurements show that the instability occurs due to non-normal mode bifurcation, which sensitively depends on initial conditions [15] including disturbances. It is revealed in different CSs observed in two cases: only streaks for small perturbations versus rolls and streaks for strong ones. Moreover, in the current case, besides the perturbations from inlet generated stream-wise elastic waves, six holes along the channel further support the elastic waves by pumping energy. It is clearly characterized by measurements of their attenuation along the channel, of which details

will be published elsewhere. On other hand, the current case has a reduced intensity of elastic waves that results in the absence of the secondary instability in streaks, namely the Kelvin-Helmholtz-like elastic instability discovered recently in a channel viscoelastic flow with strong perturbations [24].

We are grateful to Guy Han and Rostyslav Baron for their help with the experimental setup. This work was partially supported by grant from the Israel Scientific Foundation (ISF, grant #784/19.)

- 
- [1] R. G. Larson, Eric S. G. Shaqfeh, and S. J. Muller. A purely elastic instability in taylor-couette flow. *Journal of Fluid Mechanics*, 218:573–600, 1990.
  - [2] Eric SG Shaqfeh. Purely elastic instabilities in viscometric flows. *Annual Review of Fluid Mechanics*, 28(1):129–185, 1996.
  - [3] A Fouxon and V Lebedev. Spectra of turbulence in dilute polymer solutions. *Physics of Fluids*, 15(7):2060–2072, 2003.
  - [4] Alexander Groisman and Victor Steinberg. Elastic turbulence in a polymer solution flow. *Nature*, 405(6782):53–55, 2000.
  - [5] Victor Steinberg. Elastic turbulence: An experimental view on inertialess random flow. *Annual Review of Fluid Mechanics*, 53(1):27–58, 2021.
  - [6] Peyman Pakdel and Gareth H McKinley. Elastic instability and curved streamlines. *Physical Review Letters*, 77(12):2459, 1996.
  - [7] VA Gorodtsov and AI Leonov. On a linear instability of a plane parallel couette flow of viscoelastic fluid. *Journal of applied mathematics and mechanics*, 31(2):310–319, 1967.
  - [8] Michael Renardy and Yuriko Renardy. Linear stability of plane couette flow of an upper convected maxwell fluid. *Journal of Non-Newtonian Fluid Mechanics*, 22(1):23–33, 1986.
  - [9] Robert Byron Bird, Robert Calvin Armstrong, and Ole Hassager. *Dynamics of polymeric liquids. Vol. 1: Fluid mechanics*. Wiley, 1987.
  - [10] Alexander N Morozov and Wim van Saarloos. Subcritical finite-amplitude solutions for plane couette flow of viscoelastic fluids. *Physical review letters*, 95(2):024501, 2005.
  - [11] Nazish Hoda, Mihailo R Jovanović, and Satish Kumar. Energy amplification in channel flows of viscoelastic fluids. *Journal of Fluid Mechanics*, 601:407–424, 2008.
  - [12] Mihailo R Jovanović and Satish Kumar. Nonmodal amplification of stochastic disturbances in strongly elastic channel flows. *Journal of non-newtonian fluid mechanics*, 166(14-15):755–778, 2011.
  - [13] Binh K Lieu, Mihailo R Jovanović, and Satish Kumar. Worst-case amplification of disturbances in inertialess couette flow of viscoelastic fluids. *Journal of Fluid Mechanics*, 723:232–263, 2013.
  - [14] Jacob Page and Tamer A Zaki. Streak evolution in viscoelastic couette flow. *Journal of fluid mechanics*, 742:520–551, 2014.
  - [15] Peter J Schmid. Nonmodal stability theory. *Annu. Rev. Fluid Mech.*, 39:129–162, 2007.
  - [16] Lloyd N Trefethen, Anne E Trefethen, Satish C Reddy, and Tobin A Driscoll. Hydrodynamic stability without eigenvalues. *Science*, 261(5121):578–584, 1993.
  - [17] Fabian Waleffe. On a self-sustaining process in shear flows. *Physics of Fluids*, 9(4):883–900, 1997.
  - [18] W Schoppa and Fazle Hussain. Coherent structure generation in near-wall turbulence. *Journal of fluid Mechanics*, 453:57–108, 2002.
  - [19] Daniel Bonn, François Ingremau, Yacine Amarouchene, and Hamid Kellay. Large velocity fluctuations in small-reynolds-number pipe flow of polymer solutions. *Physical Review E*, 84(4):045301, 2011.
  - [20] L Pan, A Morozov, C Wagner, and PE Arratia. Non-linear elastic instability in channel flows at low reynolds numbers. *Physical review letters*, 110(17):174502, 2013.
  - [21] Boyang Qin and Paulo E Arratia. Characterizing elastic turbulence in channel flows at low reynolds number. *Physical Review Fluids*, 2(8):083302, 2017.
  - [22] Boyang Qin, Paul F Salipante, Steven D Hudson, and Paulo E Arratia. Flow resistance and structures in viscoelastic channel flows at low re. *Physical review letters*, 123(19):194501, 2019.
  - [23] Narsing K. Jha and Victor Steinberg. Universal coherent structures of elastic turbulence in straight channel with viscoelastic fluid flow, 2020.
  - [24] Narsing K Jha and Victor Steinberg. Elastically driven kelvin-helmholtz-like instability in straight channel flow. *Proceedings of the National Academy of Sciences*, 118(34), 2021.
  - [25] Ron Shnapp and Victor Steinberg. Non-modal elastic instability and elastic waves in weakly perturbed channel flow, 2021.
  - [26] Yonggang Liu, Yonggun Jun, and Victor Steinberg. Concentration dependence of the longest relaxation times of dilute and semi-dilute polymer solutions. *Journal of Rheology*, 53(5):1069–1085, 2009.
  - [27] Alex Liberzon, Theo Käufer, Andreas Bauer, Peter Vennemann, and Erich Zimmer. Openpiv/openpiv-python: Openpiv-python v0.23.3, Sep 2020.
  - [28] Philip G Drazin and William Hill Reid. *Hydrodynamic stability*. Cambridge university press, 2004.
  - [29] Gokul Hariharan, Mihailo R Jovanović, and Satish Kumar. Localized stress amplification in inertialess channel flows of viscoelastic fluids. *Journal of Non-Newtonian Fluid Mechanics*, 291:104514, 2021.
  - [30] Mihailo R Jovanović and Satish Kumar. Transient growth without inertia. *Physics of Fluids*, 22(2):023101, 2010.
  - [31] Atul Varshney and Victor Steinberg. Elastic alfven waves in elastic turbulence. *Nature communications*, 10(1):1–7, 2019.